Available online at www.sciencedirect.com
ScienceDirect
Mechanical Systems and Signal Processing 22 (2008) 374–389
Mechanical Systems and Signal Processing
www.elsevier.com/locate/jnlabr/ymssp

Numerical simulation and experimental study of a two-stage reciprocating compressor for condition monitoring

M. Elhaj[a], F. Gu[b,*], A.D. Ball[b], A. Albarbar[a], M. Al-Qattan[b], A. Naid[a]

[a]*Health Monitoring and Through Life Support Research Group, School of Mechanical, Aerospace and Civil Engineering, University of Manchester, Oxford Road M13 9PL, Oxford, UK*
[b]*School of Computing and Engineering, The University of Huddersfield, Queensgate, Huddersfield HD1 3DH, UK*

Received 27 October 2006; received in revised form 3 August 2007; accepted 6 August 2007
Available online 14 August 2007

Abstract

A numerical simulation of a two-stage reciprocating compressor has replicated the operations of the compressor under various conditions for the development of diagnostic features for predictive condition monitoring. The simulation involves the development of a mathematical model of five different physical processes: speed–torque characteristics of an induction motor, cylinder pressure variation, crankshaft rotational motion, flow characteristics through valves and vibration of the valve plates. Modelling both valve leakage and valve spring deterioration has also been achieved. The simulation was implemented in a MATLAB environment for an efficient numerical solution and ease of result presentation. For normal operating conditions, the simulated results are in good agreement with the test results for cylinder pressure waveforms and crankshaft instantaneous angular speed (IAS). It has been found that both the IAS fluctuation and pressure waveform are sensitive detection features for compressor faults such as valve leakage and valve spring deterioration. However, IAS is preferred because of its non-intrusive measurement nature. Further studies using the model and experiments are being undertaken in order to develop fault detection features for compressor driving motors and transmission systems.

Keywords: Reciprocating compressor; Numerical simulation; Instantaneous angular speed; Cylinder pressure; Condition monitoring

1. Introduction

Reciprocating compressors are one of the most popular machines in use in industry. The effective and accurate diagnosis of possible faults which degrade compressor performances are required to help in both reducing maintenance costs and increasing the plant efficiency. For these requirements, a large amount of research work has been conducted with state of the art technologies in detecting and diagnosing various faults in reciprocating compressors. Liang et al. [1] developed a procedure for the detection and diagnosis of valve faults using vibration in the time domain, frequency domain and smoothed-pseudo-Wigner–Ville-distribution. Gu et al. [2] studied automating the diagnosis of valve faults in reciprocating compressors. In 1984, Imaichi et al. [3] studied vibration sources in reciprocating compressors and how to minimise vibration generation.

*Corresponding author.
E-mail address: fengshou.gu@man.ac.uk (F. Gu).

0888-3270/$ - see front matter © 2007 Elsevier Ltd. All rights reserved.
doi:10.1016/j.ymssp.2007.08.003

Daniel et al. [4] focused on vibration and dynamic pressure methods, including the P–V diagram, for fault diagnosis and condition monitoring of reciprocating compressors. Elhaj et al. [5] developed a new method for the monitoring and diagnosis of valve faults in reciprocating compressors using the features obtained from the time domain, frequency domain and continuous wavelet transform of the airborne sound signals.

To develop more accurate fault detection methods, many investigations have been carried out on developing mathematic models of compressors. Costagliola [6] developed the first mathematical model of a reciprocating compressor. The main concern in this model was the dynamics of the valves. The modelled valves were reed type and only one degree of freedom was presumed. Wambasganss [7] worked with a similar model, a high-speed hermetically sealed compressor fitted with reed valves. As with Costagliola's model, Wambasganss paid special attention to the dynamics of the valves; however, several degrees of freedom were allowed. Manepatil et al. [8] studied the modelling and computer simulation of reciprocating compressors with various faults incorporated, as to determine the influence of the faults on performance parameters, using pressure signals to detect and quantify the faults.

There are two significant advantages of employing a mathematical model and a simulation study. One is that with their help less time and equipment are needed to obtain effective fault signatures, especially for the faults, which cannot be induced to a real machine for test studies. The other one is that it permits the researchers to examine the performance of different compressors over the same operating conditions [9,10]. Because of these advantages, this study uses them to develop the detection features for reciprocating compressors. In addition to studying the features from pressure measurement, this paper also investigates crankshaft instantaneous angular speed (IAS) for fault detection. One of the merits of IAS measurement is that it is non-intrusive, compared with the pressure measurement. IAS also has less noise contamination and is more directly related to machine dynamics, compared with conventional structural vibration and airborne acoustics. Therefore, it is easier to interpret IAS results and produce more accurate diagnoses. In addition, the encoder used for IAS measurement is not only cheaper, but also does not need periodic calibration. This allows for the accurate comparison of measurements in different periods and different IAS sensors. For these merits, IAS measurement-based monitoring has studied widely in recent years [17].

Therefore, this paper develops a mathematical model for a two-stage reciprocating compressor to simulate different operations including normal and faulty compressor conditions. It models the working process with a number of non-linear, coupled with differential equations describing the crank mechanism, valve movement, and discharge processes for both the low- and high-pressure compressor cylinders. Simulations are then conducted under different operating and fault conditions including the effects of load change due to change in discharge pressure, and valve faults such as leaking valves. To identify the fault features from both cylinder pressures and crankshaft IAS the simulated and measured results are represented in the angular domain so that they can be explored in association with the typical events in a compressor working cycle. In addition, a test system is also developed to evaluate the model and the simulated results through waveform comparisons between the measured and the predicted pressures and IAS.

2. Dynamic modelling of a two-stage reciprocating compressor

A reciprocating compressor driven by an electric motor converts electric energy into potential energy of the compressed air through the reciprocation motion of a piston in. The working of the compressor thus consists of three different physical processes: an electromagnetic process for the electrical torque generation; a mechanical process for the dynamic movement of the crank shaft, piston and valve; and a fluid flow process for the pressure build up in the cylinders and air flow through the valve. The modelling of the compressor, therefore, focuses on these three processes, respectively.

2.1. Mechanical motion

Based on the construction and working process, a two-stage reciprocating compressor can be represented as in Fig. 1. It consists of three parts: an electric motor, a compressor unit and the compressed air storage tank.

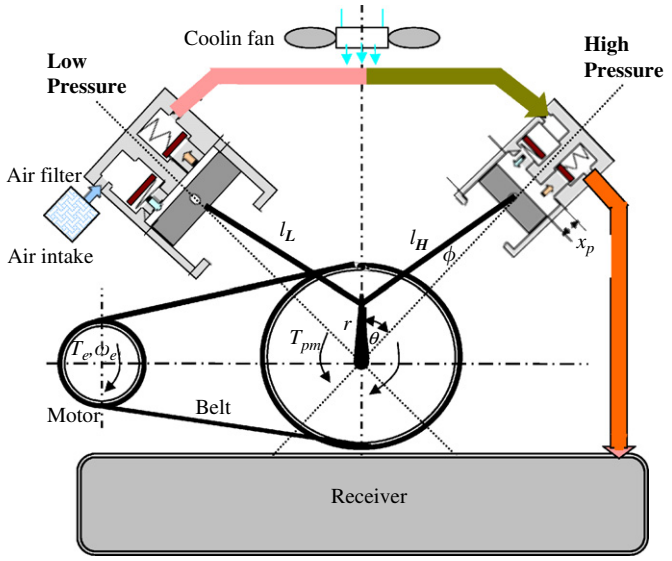

Fig. 1. Schematic and models of a two-stage compressor.

The compressor unit includes a low-pressure cylinder assembly, a high-pressure cylinder assembly, a crankshaft, a belt and a driving motor. The two pistons are driven by the torque of the crankshaft in a reciprocating motion, via a connecting rod of length l. The operating cycle is considered to commence at Top Dead Centre (TDC) of the piston in the low-pressure cylinder. From the 90° Vee-construction of the compressor, the high-pressure cylinder leads to the low-pressure cylinder by $\pi/2$. This phase difference is taken account into the equations applying to the high-pressure cylinder.

According to this simplified model, the torque balance equation of the crankshaft is

$$J\dot{\omega}(t) = T_m(t) - T_{pm_{LH}}(t) - T_{f_{LH}}(t), \tag{1}$$

where the subscripts c, i, d refer to the cylinder, inlet and discharge, respectively, the lower subscripts LH means that the expression is valid for both the low- and high-pressure cylinders, which are also referred to as the first and second stage, respectively. J is the moment of inertia of the power unit (consisting of the reciprocating parts, rotating parts of the compressor, an electric motor rotor and a power transmission shaft or a belt connected to the motor and compressor). $T_m(t)$ is the driving torque from the electric motor. $T_{pm_{LH}}(t) = T_{pm_L} + T_{pm_H}$ is the resultant torque due to the air pressure inside the cylinders and the reciprocating inertial force of the pistons, the connecting rods for both the first and second stages. $T_{f_{LH}}(t)$ is the frictional torque for the whole machine.

For either the low- or high-pressure stage, it can be shown that the resultant torque due to the air pressure inside the cylinder and the inertial force of the piston and the connecting rod is [11]

$$T_{pm} = (f_p + f_m)r, \tag{2}$$

where f_p is the tangential force produced by the air pressure in the cylinder, f_m is the tangential force produced by the inertia of the reciprocating mass; and r is the radius of the crank. The tangential force produced by the air pressure in a cylinder can be obtained by

$$f_p = p_c s_c \left(\sin\theta + \cos\theta \frac{(r/l)\sin\theta}{\sqrt{1-(r/l)^2\sin^2\theta}} \right), \tag{3}$$

where p_c is the pressure in cylinder, $s_c = 0.25\pi d^2$ is the cross-sectional area of the cylinder and d is the bore diameter of the cylinder. The tangential force produced by the vertical inertial force for both

cylinders becomes

$$f_m = -m_{\text{rec}}\ddot{x}_p\left(\sin\theta + \cos\theta\frac{(r/l)\sin\theta}{\sqrt{1-(r/l)^2\sin^2\theta}}\right). \tag{4}$$

The reciprocating mass of both stages m_{rec} is calculated from the following equation:

$$m_{\text{rec}} = m_p + 0.5m_{cr}, \tag{5}$$

where m_p is the piston mass and m_{cr} is the equivalent reciprocating mass of the connecting rod. The piston acceleration $\ddot{x}_p$ can be obtained based on the dynamics of piston motion. Taking the TDC as the reference position, as shown in Fig. 1, the displacement of the piston in the cylinder is

$$x_p = x_0 + r(1 - r\cos\theta) + l\left[1 - \sqrt{1-(r/l)^2\sin^2\theta}\right], \tag{6}$$

where x_0 is the clearance distance between the piston and the cylinder head at TDC. The velocity and acceleration of the pistons can be obtained by differentiating with respect to time:

$$\dot{x}_p = \omega r\sin\theta(1 + r/l\cos\theta)/\sqrt{1-(r/l)^2\sin^2\theta}. \tag{7}$$

Since the squared term $(r/l)^2\sin^2\theta \ll 1$, the acceleration can then be simplified as

$$\ddot{x}_p = \omega^2 r(\cos\theta + r/l\cos 2\theta). \tag{8}$$

2.2. Speed–torque characteristics of an induction motor

The speed–torque characteristics of an induction motor can be obtained through a complicated model describing the electromagnetic relationship between the stator and the rotor. For computational efficiency but incorporating the dynamic effect during the steady-state operation, a linear approximation around the rating points of the motor is introduced to describe the relationship between the motor speed and its output torque. Ignoring the elastic deformation of the belt, the motor torque applied to the shaft can be modelled as

$$T_m = T_r(1 - k(\omega_r - \Delta\omega_r)), \tag{9}$$

where T_r and ω_r are the average torque and speed of the crank shaft, respectively, which relate to the rating torque and speed of the motor by considering the transmission ratio B_r i.e.

$$T_r = \frac{P_e}{\omega_e}B_r, \tag{10}$$

$$\omega_r = \frac{\omega_e}{B_r}, \tag{11}$$

where P_e and ω_e in Eqs. (10) and (11) are the rating power and speed of the motor, respectively.

The parameters k and $\Delta\omega_r$ reflect the degree of speed fluctuation of the crankshaft and hence the possible torque fluctuation. For the motor used in this study, they were determined by measuring the speed variation of the motor with the tank pressure. At a high tank pressure, the motor is loaded with a high torque and hence runs at a slightly lower speed. While at a low tank pressure, the motor runs at a slightly higher speed. Based on this and the measurements, the speed change rate with load was estimated around the rating operating condition.

2.3. Cylinder pressure

Assuming that the process is isentropic and air is of ideal gas, the equation for the cylinder pressure $p_{c_{LH}}$ can be derived from the first law of thermodynamics [4] as

$$\dot{p}_{c_{LH}} = \frac{1}{v_{c_{LH}}}\left[c^2_{i_{LH}}\dot{m}_{vi_{LH}} - c^2_{c_{LH}}\dot{m}_{vd_{LH}} - \gamma p_{c_{LH}}\dot{v}_{c_{LH}}\right], \tag{12}$$

where the variable cylinder volume $v_{c_{LH}}$ can be determined by the clearance volume and piston motion:

$$v_{c_{LH}} = v_{co_{LH}} + s_{c_{LH}} x_{p_{LH}}, \tag{13}$$

$\dot{m}_{vi_{LH}}$ and $\dot{m}_{vd_{LH}}$ are the mass flow rates through the inlet and discharge valves, respectively. $\gamma = 1.4$ is the ratio of specific heats. $c^2_{i_{LH}} = \gamma R T_{i_{LH}}$ is the squared speed of sound in the inlet plenum, and $c^2_{c_{LH}} = \gamma R T_{c_{LH}}$ is the squared speed of sound in the cylinder. $v_{co_{LH}}$ is the clearance volume, R is the gas constant for air, and D_{LH} is the cylinder diameter.

If the gas is assumed to undergo an isentropic process, there is no heat transfer to the surroundings. As a result, the temperature must be variable at different stages of the compression process, which can be calculated:

$$T_{c_{LH}} = T_{i_{LH}} \left(\frac{p_{c_{LH}}}{p_{i_{LH}}} \right)^{(\gamma-1)/\gamma}, \tag{14}$$

where $p_{c_{LH}}$ is the cylinder pressure, $p_{i_{LH}}$ the inlet pressure, and $T_{i_{LH}}$ the average absolute temperature of the inlet air (i.e. the atmospheric temperature for the low-pressure stage). The change rate of the cylinder volume $v_{c_{LH}}$ can be determined using geometric parameters and the velocity of piston:

$$\dot{v}_{c_{LH}} = s_{p_{LH}} \dot{x}_{p_{LH}}. \tag{15}$$

2.4. Mass flow through valves

The mass flow rate $\dot{m}_{vd_{LH}}$ through the discharge valve is modelled as incompressible flow through an orifice:

$$\dot{m}_{vd_{LH}} = \beta_{d_{LH}} C_{dd_{LH}} A_{fd_{LH}} \sqrt{2\rho_{c_{LH}} |p_{d_{LH}} - p_{c_{LH}}|}, \tag{16}$$

where $\beta_{d_{LH}} = \text{sign}(p_{d_{LH}} - p_{c_{LH}})$ is the flow direction parameter: $+1$ for normal flow from cylinder to discharge passage while -1 for possible backflow from discharge passage to the cylinder, $p_{d_{LH}}$ is the pressure in the discharge plenum, $A_{fd_{LH}}$ is the maximum flow area of the discharge valve, $C_{dd_{LH}}$ is a variable discharge coefficient which accounts for the reduced flow area resulting from the separated flows and changes with the valve lift according to [12], and $\rho_{c_{LH}} = \rho_{\text{ref}} (p_{c_{LH}}/p_{\text{ref}})^{1/\gamma}$ is the density of the air in the cylinder, which is derived from isentropic flow.

In the same way, the mass flow rate through the inlet valve can be expressed as

$$\dot{m}_{vi_{LH}} = \beta_{i_{LH}} C_{di_{LH}} A_{fi_{LH}} \sqrt{2\rho_{c_{LH}} |p_{i_{LH}} - p_{c_{LH}}|}, \tag{17}$$

where each symbol means the same as that of Eq. (16) but for the discharge valve rather than the inlet valve.

2.5. Valve motion

Each cylinder has two valves: inlet and discharge. These two valves have similar construction and can be modelled as a non-linear vibration impact system [2,5,13], as illustrated in Fig. 2.

Driven by the force due to the gas pressure, the valve plate goes through a sequence of events: the opening of the valve, the impact between the valve and the upper seat, the closing of the valve, and the impact between the valve and the lower seat. The equation of motion for inlet valves are in the opening and closing of the valve, when $0 \leqslant x_{vs} < x_{vs\,\max}$, is

$$m_{vs_{LH}} \ddot{x}_{vs_{LH}} + c_{s_{LH}} \dot{x}_{vs_{LH}} + k_{vs_{LH}} x_{vs_{LH}} = \Sigma f_{vs_{LH}}. \tag{18}$$

When the valve plate comes into contact with the valve seats (the valve is totally open or totally closed), $0 \leqslant x_{v_{LH}}$ or $x_{v_{LH}} \geqslant x_{vs\,\max}$, impacts occur and can be described by

$$m_{vs_{LH}} \ddot{x}_{vs_{LH}} + c_{s_{LH}} \dot{x}_{vs_{lh}} + k_{vs_{LH}} x_{vs_{LH}} + c_{cs_{LH}} \dot{x}_{vs_{lh}} + k_{cs_{LH}} x_{vs_{LH}} = \Sigma f_{vs_{LH}}, \tag{19}$$

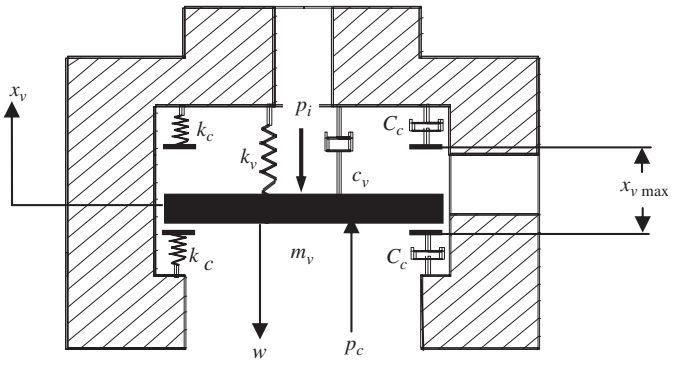

Fig. 2. Vibro-impact model of compressor valve.

where $\ddot{x}_{vs_{LH}}$, $\dot{x}_{vs_{LH}}$, and $x_{vs_{LH}}$ are the valve plate acceleration, velocity and displacement, respectively, $m_{vs_{LH}}$ is the equivalent mass of the inlet valve plate, $c_{s_{LH}}$ is the damping coefficient, $k_{vs_{LH}}$ is the non-linear spring stiffness while the valve moves between the valve seats, $k_{cs_{LH}}$ is the contact stiffness between seat and valve plate for both stages, $c_{cs_{LH}}$ is the contact damping coefficient, and $\Sigma f_{vs_{LH}}$ is the resultant force acting on the valve plate.

The equivalent mass is the valve plate mass plus one-third of the mass of the valve spring:

$$m_{vs_{LH}} = m_{\text{plate}} + \tfrac{1}{3} m_{\text{spring}}. \tag{20}$$

The damping coefficient is calculated by

$$c_{s_{LH}} = 2\xi\sqrt{k_{vs_{LH}} m_{vs_{LH}}}, \tag{21}$$

where ξ is the damping ratio of the valve unit and can be estimated by observing the oscillations of the cylinder pressure measured.

The resultant force on the valve is from three forces: weight of valve $w_{sv_{LH}}$, the preset spring force $f_{svo_{LH}}$ and the force due to pressure difference between each side of the valve $c_f s_{sv_{LH}}(p_{i_{LH}} - p_{c_{LH}})$, and is calculated by

$$\Sigma f_{vs_{LH}} = -w_{sv_{LH}} + f_{svo_{LH}} - c_f s_{sv_{LH}}(p_{i_{LH}} - p_{c_{LH}}), \tag{22}$$

where c_f is a force coefficient changing with the valve's lift, to take account of the pressure drop across the valve [14,15], $s_{sv_{LH}}$ is the slot area for a single channel, $p_{c_{LH}}$ is the cylinder pressure, and $p_{i_{LH}}$ is the pressure in the respective inlet plenum.

Similarly, the equation of motion of the discharge valve can be obtained in the same form as Eqs. (18) and (19).

2.6. Implementation of the simulation

To explore the relationship between different process parameters for condition monitoring, a simulation program has been developed in MATLAB to solve the equations numerically. The core part of the program is to solve the differential equations. In this study, an explicit Runge–Kutta formula was used in solving the equations and the desired accuracy was controlled by adjusting the step size and the error parameters through the routine provided in MATLAB.

The equations solved include Eq. (1) to obtain the instantaneous angular speed of the crank shaft; two sets of Eq. (12) to obtain the instantaneous pressures in both the low-pressure cylinder and the high-pressures cylinder; and four sets of Eq. (18) to get the valve motion of the inlet and discharge processes at both the low- and high-pressure stages. All the solutions are represented in the time domain or angular domain. By investigating the variations of the time domain waveforms between different operating conditions, including the abnormal typical fault conditions, representative monitoring features are developed. These features are easier to interpret using common engineering knowledge, compared with interpretation of features commonly used in the frequency domain.

For the solution of the equations, the TDC of the low-pressure stage is taken as the initial point. The initial conditions including the crankshaft speed, cylinder pressures and valve displacement are set to be the nominal values estimated based the TDC positions. In particular, the initial pressure value for the low-pressure stage is near to its maximum while it should be the minimum for the high-pressure stage. In this way the solving process has small transient errors and converges to the required accuracy quickly.

In addition, the damping ratio for valve system and the moment of crankshaft inertia are tuned to more accurate values through a number of trial simulations. These parameters are difficult to be measured accurately because the complexity of the construction and possible vortex flow in the valve chamber. By combining the predicted pressure waveforms and the IAS waveform with their measured counterparts, these parameters are adjusted so that the predictions agree to the measurements as closely as possible.

3. Experimental system

A Broom–Wade (Model TS9) reciprocating air compressor was used for the simulation and experimental study. The compressor consists of a two-stage air intensifier with an air-cooling system as shown in Fig. 3. A three-phase induction motor drives the compressor to run at a speed of 425 rpm [17]. The details of the system are provided in Appendix A.

For the experimental study, the compressor is fully instrumented with several different sensors and a measurement system. An optical shaft encoder is attached to the crankshaft, shown in Fig. 3 for the IAS measurement and the indication of the TDC of the lower pressure stage. Two pressure transducers are mounted into the first and the second cylinder, respectively, to measure the cylinder pressure waveforms. In addition, two accelerometers and two microphones are also used to get the vibrations and acoustics for vibro-acoustic-based monitoring study, which is not covered in this paper.

The measurement system shown in Fig. 4 is comprised of a high-performance ADC (16 channel, 400 kHz sampling rate and 16 bit data resolution) device and a PC. The software on the PC controls the data acquisition process to acquire data at the specified discharge pressure values: 0.27, 0.54, and 0.82 MPa, and the defined angular positions. During the tests, the system measures continuously the static discharge pressure in the storage tank and the temperatures of the cylinder block. When the tank pressure reaches a predefined value the measurement system triggers the dynamic data acquisition to record the cylinder pressure and IAS data for a segment of 1.2 s. In this way the data acquisition is fully automated, which guarantees the alignments of each data segment and hence allows subsequent comparative studies to be made accurately between different tests.

The IAS data acquired from the shaft encoder is a train of square waves modulated by variations in the speed signal. To obtain the IAS waveform of interest, an FFT-based algorithm [16–18] is used to demodulate the waveform from the square wave train. Comparing with the conventional pulse counting method for IAS

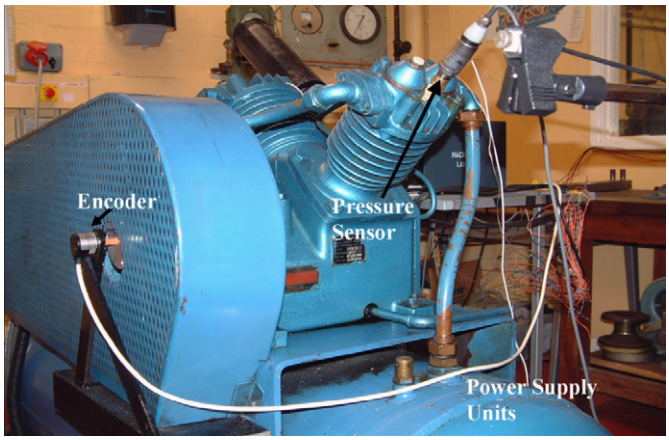

Fig. 3. Two-stage reciprocating compressor.

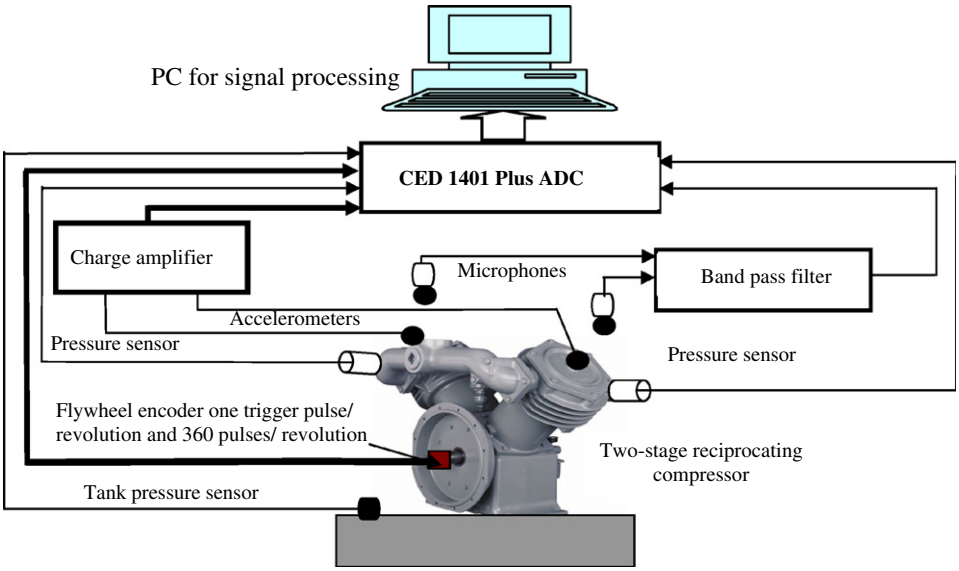

Fig. 4. Schematic of reciprocating compressor test system.

extraction, this algorithm provides a higher accuracy in IAS estimation. As the changes of IAS variations in the reciprocating compressor is small, particularly when it is running under small fault conditions, the high accuracy allows a better differentiation to be achieved for fault detection and diagnosis.

4. Model evaluation

To evaluate the developed model, both the measured and predicted results are presented for a complete work cycle in the angular domain. It allows a direct comparison of the results to be made over the compressor operating processes: suction, compression, discharge and expansion. The cylinder pressures and crankshaft IAS are focused on in the comparison, as they are the major parameters describing the dynamics of a compressor.

4.1. Comparison of measured and predicted cylinder pressures

Fig. 5 shows the measured and predicted cylinder pressure for both stages. For the low-pressure stage, both the predicted and measured pressure waveforms, Fig. 5(a) shows the four working processes clearly. A rapid drop in cylinder pressure during re-expansion can be seen in the angular range from 0° to 22° as the piston moves down the cylinder. When the cylinder pressure drops sufficiently below that of the inlet manifold (0.1 MPa), the inlet valve opens and air enters the cylinder during the suction process, which lasts from 22° to 190°. After bottom dead centre, the air inside the cylinder is compressed as the piston moves upwards, producing a rapid pressure rise in the cylinder. When the cylinder pressure exceeds that of the discharge manifold by a sufficient amount, the discharge valve opens and the cylinder discharges, this process occurs from around 270–360°. Following this a new operating cycle starts.

The high-pressure stage also works following the four processes above, but each corresponding process occurs 90° earlier in terms of crank position. This shift leads to the high-pressure cylinder suction process lying just within the discharge process of the low-pressure stage. In such a way, the high-pressure cylinder can be fully charged at a higher pressure than would otherwise be possible. The combined effects of the two stages produce a large pressure increase as shown by the pressure amplitude of the final discharge in Fig. 5(b).

Comparing the measured and predicted pressures, the simulated results are found to be good agreement with the test results for both the low and high-pressure cylinders. This confirms that the pressure model is reliable and the parameters are tuned to the appropriate values. Admittedly, the measured pressure traces

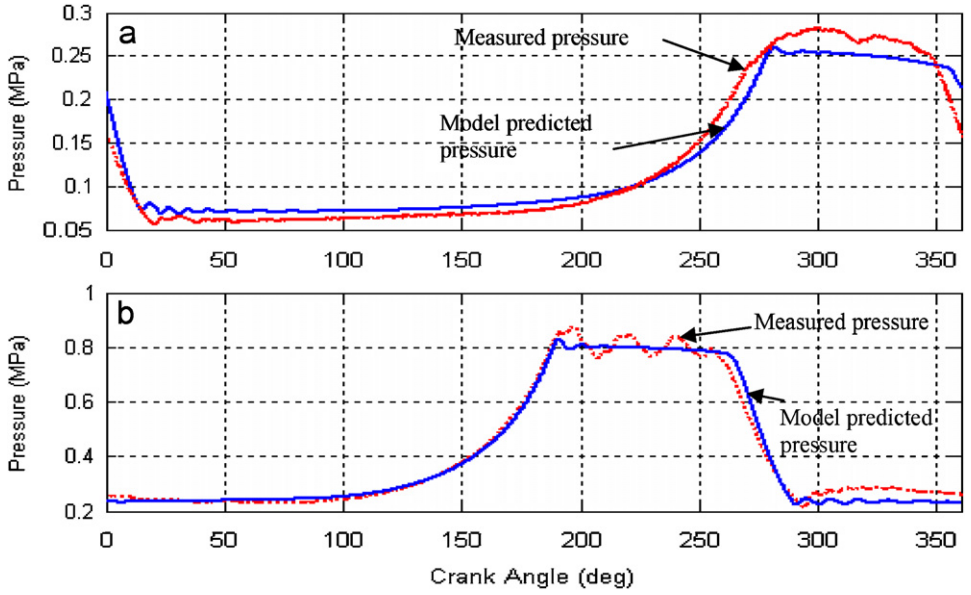

Fig. 5. Comparison of experimental and predicted pressure signals: (a) low-pressure cylinder; (b) high-pressure cylinder at discharge pressure 0.82 MPa.

show slight oscillations, particularly in the high-pressure cylinder, and these are likely due to the combined influences of valve flutter and resonance of the valve chamber. Because the oscillation amplitude is relatively small, such effects will have little influence on the IAS results.

4.2. Comparison between measured and predicted IAS

Figs. 6(a) illustrates the predicted waveform of IAS over a compressor cycle under three the discharge pressures: 0.27, 0.54, and 0.82 MPa. It can firstly be seen that the amplitude of the IAS fluctuates over the operating cycle. It can be seen to have higher amplitude in the first-half of the crank turn when the cylinder pressures of both stages have the lower amplitudes and the load to the motor is lower, while its amplitudes becomes lower in the second-half of the crank turn when the cylinder pressures are higher and motor load is higher. Especially, the IAS amplitude has two different dips corresponding to the two high-pressure regions respective to the discharge processes of the high-pressure stage and the low-pressures stage. This fluctuation demonstrates that IAS is sensitive to the in-cylinder pressure changes.

More importantly the fluctuation of IAS also varies significantly with discharge pressure. The greater the discharge pressure the more work is done by the piston in compressing the air and hence the lower the IAS amplitude. As shown in Fig. 6, for a 0.82 MPa discharge pressure the minimum IAS is 423 rpm, which is 11 rpm lower than that of 0.27 MPa discharge pressure.

Compared with the measured results shown in Fig. 7, the predicted results for both the pressures and the IAS show good consistency over different discharge conditions. This shows that this model is valid for a wide range of operating conditions and can be relied upon for fault simulation study.

5. Valve leakage detection

Leaking valves are the most common fault in reciprocating compressors. Especially, at high-pressure stages, both the inlet and discharge valves are exposed to high-speed flow, high temperature and high vibro-impacts. These harsh working conditions often result in non-uniform wear of the sealing surfaces between the valve plate and its seat, eventually causing leakage. The leakage permits high-temperature air to be forced across the valve surface by differential pressure, which further accelerates the deterioration of the valve system (including the valve spring) and reduces compressor efficiency considerably.

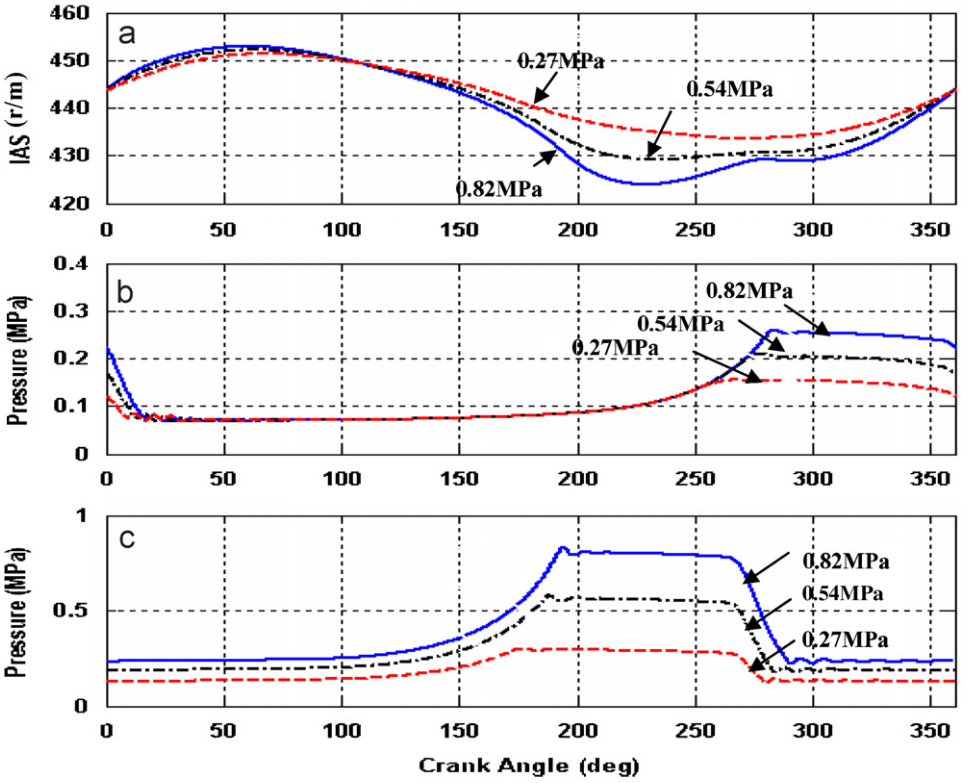

Fig. 6. Model predicted results: (a) IAS with different discharge pressures; (b) low-pressure cylinder waveform; and (c) high-pressure cylinder waveform.

5.1. Leakage modelling

Assuming there is an additional flow passage across the valve, the leakage can be simulated by drilling small hole in the valve plate. In this study a 0.8 mm diameter hole was created in the valve plate to simulate a small degree of leakage (referred to as Leak 1). As a case of larger leakage, a 1.6 mm diameter hole (refereed to as Leak 2) was created. Both of the leakage cases were introduced into the high-pressure stage where the valve works under much harsher conditions.

To take the leakage into account in the simulation process, it was modelled as an additional flow through an orifice in parallel to the normal valve flow. Specifically, the cylinder pressure in Eq. (12) was modified to include two additional mass flow terms: $\dot{m}_{iL_{LH}}$ and $\dot{m}_{dL_{LH}}$ for considering the leakages through the inlet valve and the discharge valve, respectively, i.e.

$$\dot{p}_{c_{LH}} = \frac{1}{v_{c_{LH}}}\left[c_{i_{LH}}^2 \dot{m}_{vi_{LH}} - c_{c_{LH}}^2 \dot{m}_{vd_{LH}} - \gamma p_{c_{LH}} \dot{v}_{c_{LH}} - c_{i_{LH}}^2 \dot{m}_{iL_{LH}} - c_{c_{LH}}^2 \dot{m}_{dL_{LH}}\right]. \tag{23}$$

The mass flow rate of discharge leakage $\dot{m}_{dL_{LH}}$ can be calculated based on Eq. (16) by

$$\dot{m}_{dL_{LH}} = \beta_{dL_{LH}} C_{dd_{LH}} A_{dL} \sqrt{2\rho_{c_{LH}} |p_{d_{LH}} - p_{c_{LH}}|}, \tag{24}$$

where A_{dL} is the leakage flow area of the discharge valve, $\beta_{dL_{LH}} = \text{sign}(p_{d_{LH}} - p_{c_{LH}})$ is the flow direction parameter: $+1$ for the leakage flow from the cylinder to discharge passage while -1 for leakage flow from the discharge passage back to the cylinder.

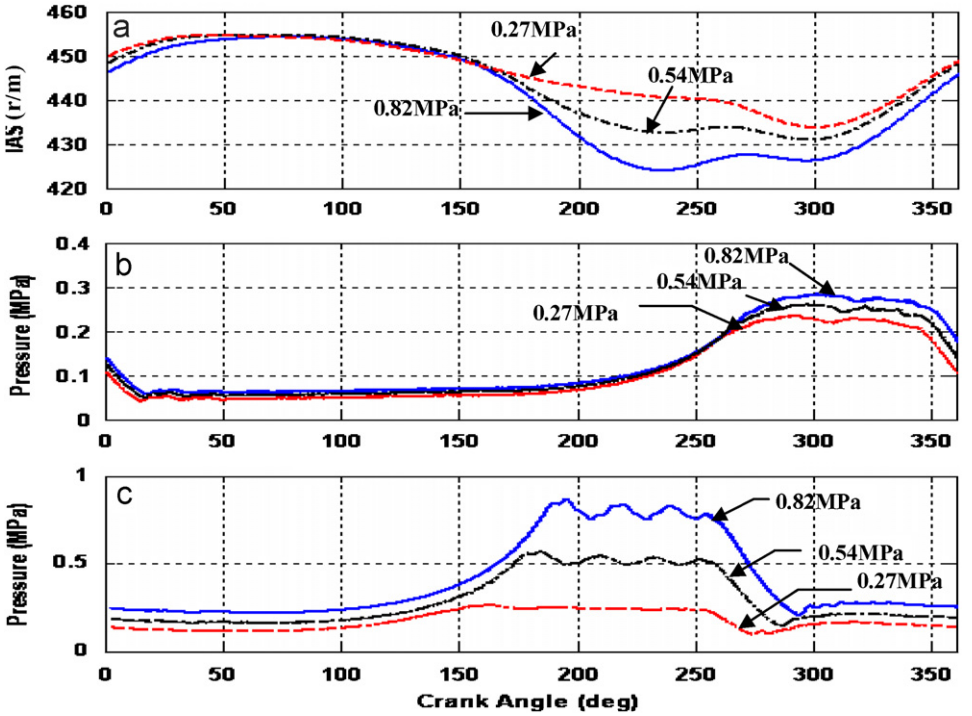

Fig. 7. Measured results: (a) IAS with different discharge pressures, (b) low-pressure cylinder waveform, and (c) high-pressure cylinder waveform.

The mass flow rate through inlet valve leakage $\dot{m}_{iL_{LH}}$ can then be calculated based on Eq. (12) by

$$\dot{m}_{iL_{LH}} = \beta_{iL_{LH}} C_{di_{LH}} A_{iL} \sqrt{2\rho_{c_{LH}} |p_{i_{LH}} - p_{c_{LH}}|}, \tag{25}$$

where A_{iL} is the leakage flow area for the inlet valve, $\beta_{iL_{LH}} = \text{sign}(p_{i_{LH}} - p_{c_{LH}})$ is the leakage direction parameter: $+1$ for the leakage flow from the cylinder to the inlet passage while -1 for leakage flow from the inlet to the cylinder.

5.2. Suction valve leakage

Fig. 8 shows the predicted results for the suction (inlet) valve leakages. Although the leakage occurs at the high-pressure stage only, the pressure waveform change occurs in both stages. In the high-pressure stage, a large deviation of the waveform is in the expansion process, corresponding to a crank angle range from 260° to 290°, as shown in Fig. 8(c). This deviation is due to back flow through the inlet leakage hole. A larger leakage causes the expansion process to occur earlier and consequently introduces a larger loss of discharge efficiency. On the other hand, the back flow also makes the pressure inside the inlet passage higher than normal. This pressure increase results in two effects: firstly, a higher inlet pressure during the suction process at the high-pressure stage and secondly an increased discharge pressure for the low-pressure cylinder, corresponding to a crank angle range from 285° to 360° shown in Fig. 8(b).

The effects of the pressure changes can be also observed in the IAS waveforms. As shown Fig. 8(a), the major changes are in the crank angle range from 285° to 340°. Because of the pressure increases during the discharge process at the low-pressure stage and during the suction process at the high-pressure stage, the IAS shows decreases in these angular positions.

All the changes in both the pressure and the IAS waveforms can also be seen from the measured results, as shown in Fig. 9. This means that the suction valve leakages can be detected not only by the pressure waveforms measured internally, but also by the IAS variations measured externally.

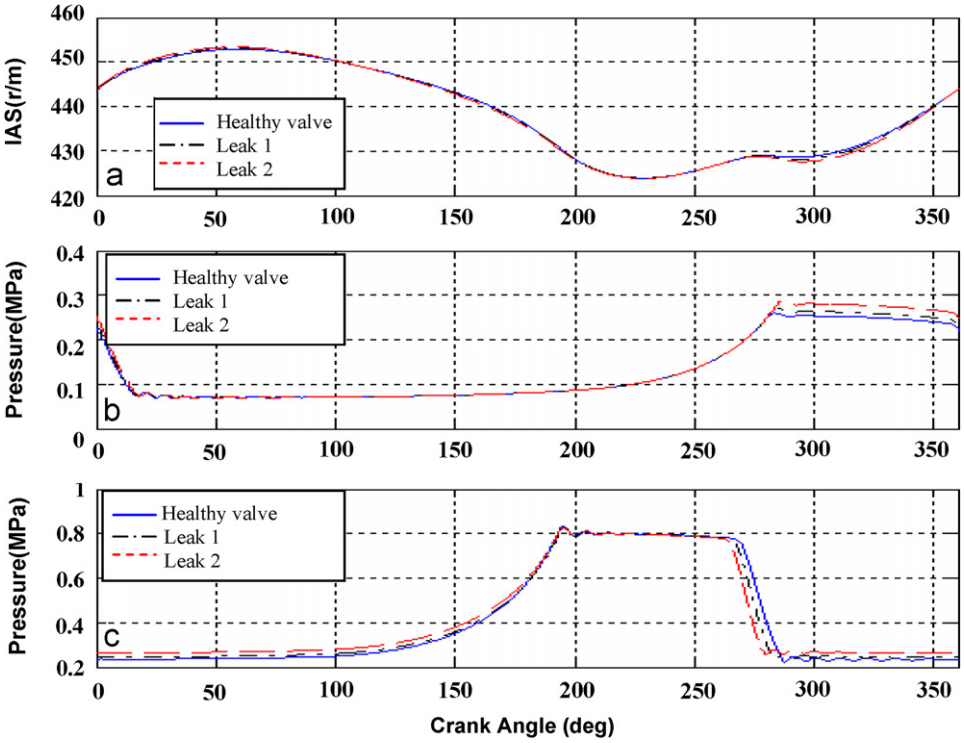

Fig. 8. Predicted results for suction valve leakage at 2nd stage.

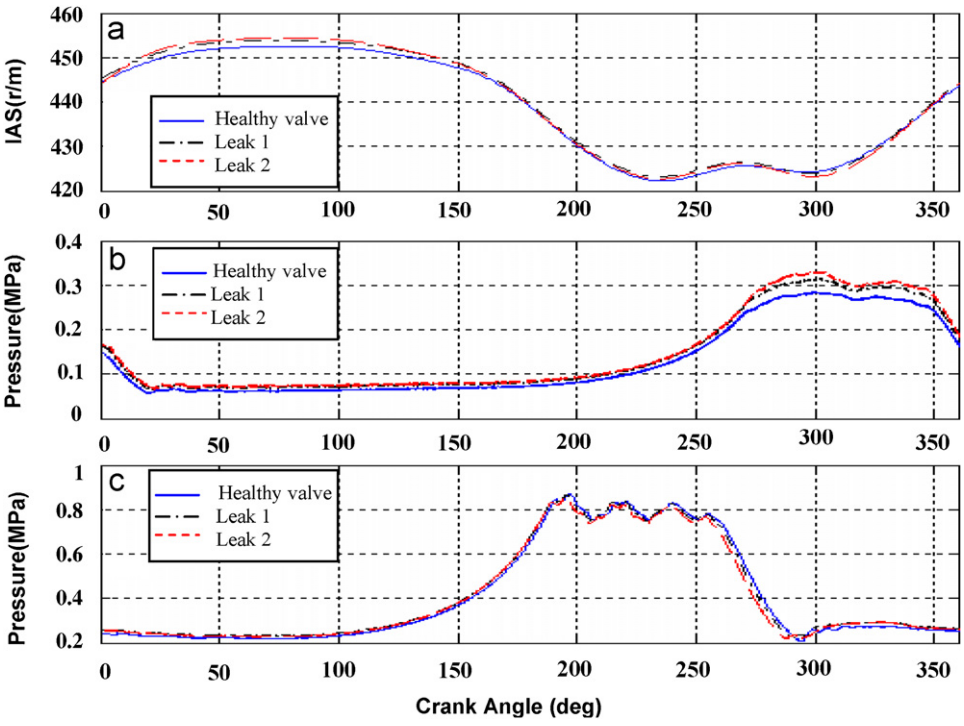

Fig. 9. Measured results for suction valve leakage at 2nd stage.

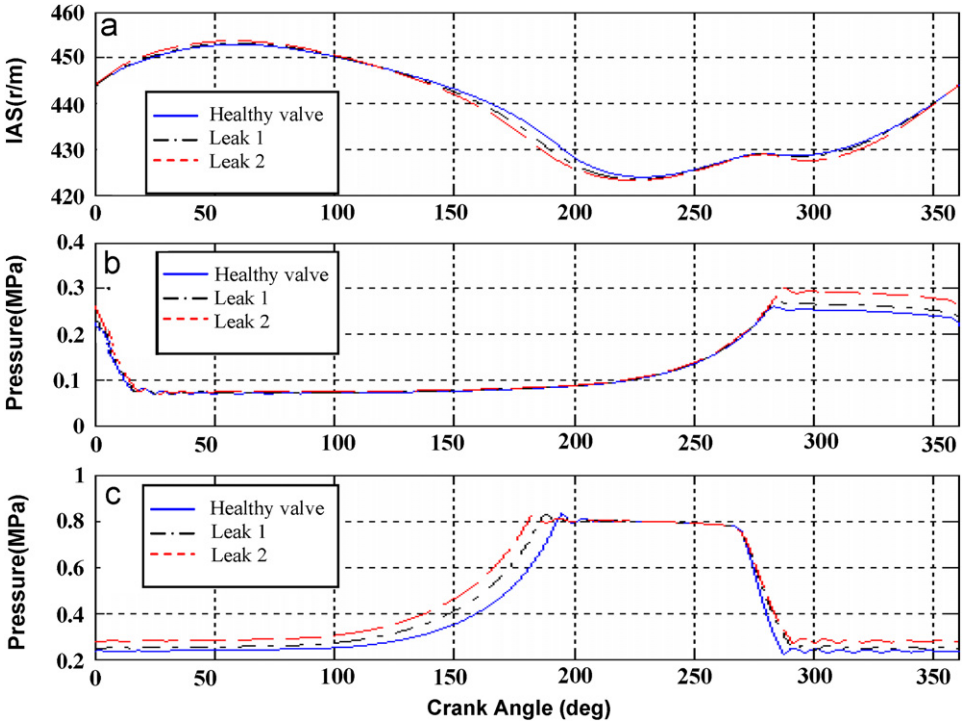

Fig. 10. Predicted results for discharge valve leakage at 2nd stage.

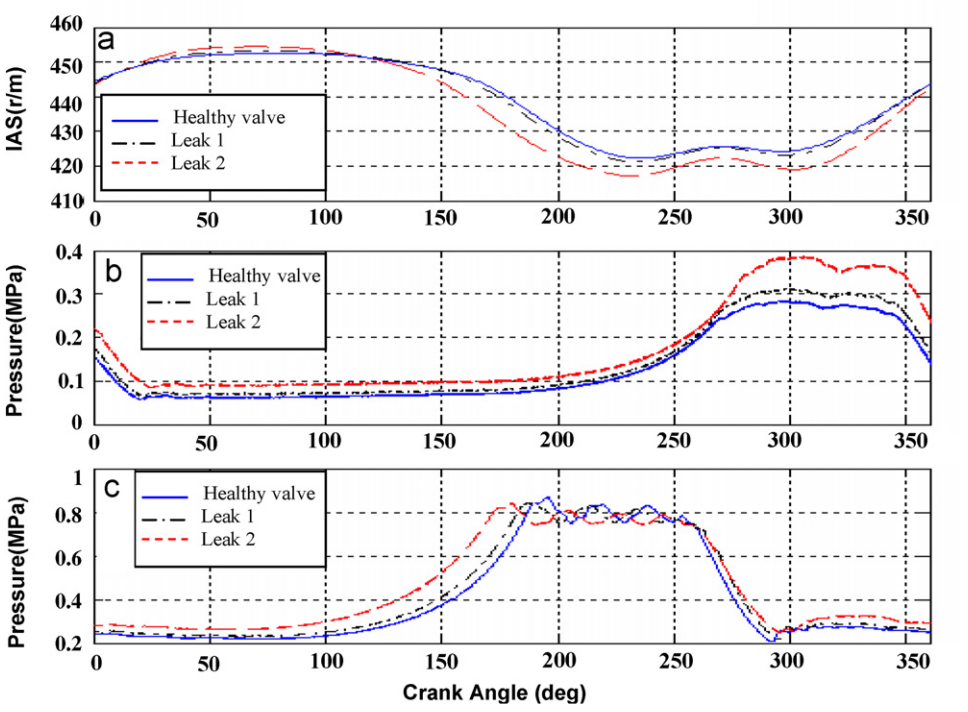

Fig. 11. Measured results for discharge valve leakage at 2nd stage.

5.3. Discharge valve leakage

Fig. 10 shows the predicted results for the discharge valve leakages. Similar to the suction leakage, the leakage occurs at the high-pressure stage causing pressure waveform changes at both stages. For the high-pressure stage, a large change occurs in the suction and compression processes, corresponding to a crank angle range from 0° to 190°, as shown in Fig. 10(c). The leakage causes cylinder pressure higher than normal and consequently the discharge process occurs much earlier. These large changes are due to the back flow through the discharge leakage hole. The larger the leakage size, the greater the leakage back into the cylinder and hence higher pressure in the suction process. The back flow also makes the pressure inside the inlet passage higher than normal, which leads to a higher discharge pressure from the low-pressure stage, corresponding to a crank angle range from 285° to 360° shown in Fig. 10(b).

The combined effects of the pressure changes can be also observed on the IAS waveforms. As shown in Fig. 10(a), a clear change is in the crank angle range from 150° to 220°. Because of the pressure increases during the compression process of the high-pressure stage, the IAS shows a decrease in these angular positions. In addition, the IAS in the crank angle range from 285° to 340° also becomes lower, which is similar to the changes in the case of inlet valve leakage due to the increase in the inlet pressure.

Test results from discharge leakage in Fig. 11 show the similar features of pressure and IAS changes revealed from the simulation results. This confirms that that the discharge valve leakages can be detected by both the pressure waveforms and the IAS fluctuation.

Furthermore, the two different leakages can be discriminated by the differences in the waveform changes. From the pressure measurements, the earlier occurrence of the expansion process can be used to detect the inlet leakage while the earlier occurrence of compression can be used for the detection of discharge leakage. In addition, the decrease in IAS around the crank angle 300° is the major symptom for inlet leakage and the decrease around 200° is for discharge leakage.

6. Conclusions

Numerical simulation and experimental study have demonstrated that IAS and cylinder pressure waveforms are capable of characterising compressor operation at different discharge pressures and under different fault conditions. Based upon these approaches fault detection methodologies can be developed for monitoring reciprocating compressors.

The mathematical model of the two-stage reciprocating compressor has been developed and evaluated by experimental results over a range of operating conditions. The close match between the predicted and measured cylinder pressure, crankshaft IAS and valve movements show that the model is reliable and accurate.

Fault simulation study shows that both the fluctuations in crankshaft IAS and cylinder pressure waveforms can be used for the detection and identification of different valve faults such as leakage in the suction and discharge plates. The pressure measurements produce a clear detection feature but it is intrusive measurement and difficult to implement. Although IAS features are not as significantly clear as those of pressure, it is of direct relevance in condition monitoring because it can be obtained non-intrusively.

Appendix A. Parameters and physical constants

A three-phase induction motor drives the compressor to run at a speed of 425 rpm [17]. The details of the system are provided in Tables A1 and A2.

Table A1
Parametric values of the TS9-16 compressor and valve systems

Compressor	
Number of cylinders	2 (90° Vee)
Compressor crank speed (rpm)	425
Motor speed (rpm)	1450
Motor power (kW)	2.24
Tank capacity (l)	272
Piston stroke (mm)	76.2
Connecting rod length and mass (mm and kg)	171.6 and 1.8
Connecting rod length and mass (mm and kg)	171.6 and 0.9
Crank radius (mm)	38.1
Piston diameter mass, low pressure (mm and kg)	93.6 and 1.78
Piston diameter and mass, high pressure (mm and kg)	55.5 and 0.89
Transmission ratio	3.1
Moment of inertia J ($kg\,m^2$)	0.41
Valve system	
Maximum inlet valve lift (mm)	2.2
Maximum discharge valve lift (mm)	2.6
Mass of valve plate, low-pressure cylinder (g)	2.3
Mass of valve plate, high-pressure cylinder (g)	2.1
Mass of valve spring, low-pressure cylinder (g)	1.0
Mass of valve spring, high pressure cylinder (g)	2.0
Outer radius valve plate, low-pressure cylinder (mm)	21.0
Outer radius valve plate, high-pressure cylinder (mm)	14.0
Discharge valve spring stiffness (N/m)	12,000
Inlet valve spring stiffness (N/m)	10,000
Equivalent contact spring stiffness (N/m)	10^7
Inner radius valve plate, low-pressure cylinder (mm)	12.5
Inner radius valve plate, high-pressure cylinder (mm)	10.5

Table A2
Air parameters

Air parameters	Low-pressure cylinder	High-pressure cylinder
Specific heat	1.4	1.4
Universal gas constant (J/kg K)	286.9	286.9
Air density (kg/m^3)	1.205	Variable
Inlet pressure (MPa)	0.10	Variable
Discharge pressure (MPa)	Variable	0.82
Inlet temperature (°C)	21	Variable
Discharge temperature (°C)	Variable	80

References

[1] B. Liang, F. Gu, A.D. Ball, A preliminary investigation of valve fault diagnosis in reciprocating compressors, Journal of Maintenance (1996) 3–8.
[2] F. Gu, A.D. Ball, Vibration based fault diagnosis in diesel fuel injection system, IMechE, Seminar on Diesel Fuel Injection Systems, London, 1995, pp. 89–97.
[3] K. Imaichi, N. Ishii, K. Imasu, A vibration source in refrigerant compressors, Journal of Vibration, Acoustic, Stress, and Reliability in Design 106 (1984) 122–128.
[4] J. Daniel, Vibration-based diagnostics of reciprocating machinery, Ph.D. Thesis, Massachusetts Institute of Technology, 1994.
[5] M. Elhaj, F. Gu, J. Wright, A.D. Ball, Early detection of leakage in reciprocating compressor valves using vibration and acoustic CWT features, in: Proceedings of the 14th International Congress on Condition Monitoring and Diagnostic Engineering Management (COMADEM), Manchester, UK, 2001, pp. 749–756.

[6] M. Costagliola, Theory of spring-loaded valves for reciprocating compressors, Journal of Applied Mechanics—Transactions of the ASME 17 (4) (1950) 415–420.
[7] M. Wasmbasganss, Mathematical modelling and design evaluation of high-speed reciprocating compressors, Ph.D. Thesis, Purdue University, 1966.
[8] S. Manepatil, G. Yadava, B. Nakra, Modelling and computer simulation of reciprocating compressor with faults, IE (I) Journal-MC, vol. 81, New Delhi, 2000, pp. 108–116.
[9] P. Rajendra, Mathematical Modelling and Simulation of Refrigerating Compressors, University of Roorkee, India, 1978.
[10] A. Roy, Mathematical modelling of reciprocating compressors for heat-pumps, Ph.D. Thesis, University of Aston, Birmingham, 1988.
[11] Y. Jianguo, P. Lijun, Fault detection in a diesel engine by analysing the instantaneous angular speed, Mechanical Systems and Signal Processing 15 (3) (2001) 549–564.
[12] G.R. Price, K.K. Botros, Numerical and experimental analysis of the flow characteristics through a channel valve, in: Purdue Compressor Technology Conference, 1992, p. 1225.
[13] O. Bardou, Early detection of leakages in the exhaust and discharge systems of reciprocating machines by vibration analysis, CETIM-Senlis, France, 1994, pp. 551–570.
[14] S. Rao, Mechanical Vibrations, third ed., Addison-Wesley, Inc., NY, USA, ISBN 0-201-59289-4, 1995.
[15] J. Fleming, A theoretical and experimental investigation of the flow of gas through reciprocating compressor valves, IMech C390/011, 1989, pp. 117–119.
[16] F. Stronach, A. Johnston, C. Cudworth, Detection of valve faults on reciprocating compressor, in: Proceeding of Condition Monitoring, Pineridge Press, 1984, pp. 293–304.
[17] F. Gu, I. Yesilyurt, Y. Li, G. Harris, A.D. Ball, An investigation of the effects of measurement noise in the use of instantaneous angular speed for machine diagnosis, Mechanical Systems and Signal Processing 20 (6) (2006) 1444–1460.
[18] Y. Li, F. Gu, A.D. Ball, N. Bennett, The measurement of instantaneous angular speed, Mechanical Systems and Signal Processing 19 (4) (2004) 786–805.